Tunable auxetic properties in group-IV monochalcogenide monolayers

Xian Kong,[1] Junkai Deng,[1,*] Lou Li,[1] Yilun Liu,[2] Xiangdong Ding,[1] Jun Sun,[1] and Jefferson Zhe Liu[3,†]

[1]*State Key Laboratory for Mechanical Behavior of Materials, Xi'an Jiaotong University, Xi'an 710049, China*

[2]*State Key Laboratory for Strength and Vibration of Mechanical Structures, School of Aerospace Engineering, Xi'an Jiaotong University, Xi'an, China 710049, People's Republic of China*

[3]*Department of Mechanical Engineering, The University of Melbourne, Parkville VIC 3010, Australia*

(Received 1 August 2018; revised manuscript received 23 September 2018; published xxxxxx)

Negative Poisson's ratio (NPR) is a counterintuitive material elastic constant that can lead to many unusual auxetic properties. Here, using first-principles calculations, we report tunable negative Poisson's ratio in the out-of-plane direction in group-IV monochalcogenide monolayers MX (M = Sn, Ge and X = S, Se). SnSe, GeS, and SnS monolayers have intrinsic NPR ν_{zx} ranging from -0.004 to -0.210 in armchair (x) tension, whereas GeSe monolayer possesses a much larger NPR ν_{zy} of -0.433 in zigzag (y) tension. Our analysis attributes the NPR effects to the relative position of M and X in the puckered structure and the smaller bending stiffness of M-X-M bond angle. We further established the correlation between electronic structures of materials and their crystal structures. It allows us to fine tune GeSe structure via electron doping, leading to a reversible and continuous change of ν_{zy} from -0.821 up to 0.895. We also demonstrate the concept of strain engineering GeSe monolayer to switch its Poisson's ratio ν_{zx} between two different values: 0.583 and -0.433. Our in-depth study provides not only fundamental knowledge but also practical routes for designing 2D smart materials with tunable negative Poisson's ratio, which are desirable for smart devices at small scale.

DOI: 10.1103/PhysRevB.00.004100

I. INTRODUCTION

Poisson's ratio is a fundamental mechanical property of materials, defined as the negative ratio of transverse strain to longitudinal strain under uniaxial tension or compression. Most materials display positive Poisson's ratio ranging from 0 to 0.5, indicating that when materials are stretched longitudinally, they tend to contract in the transverse direction [1,2]. In rare cases, materials have negative Poisson's ratio (NPR), termed as the auxetic effect [3]. They expand rather than contract laterally when stretched in the longitudinal direction. The auxetic effect endows materials with enhanced mechanical properties, including shear resistance [4], indentation resistance [5], and fracture toughness [6]. As a result, the auxetic materials have been proposed for applications in a broad range of fields, such as medicine, fasteners, tissue engineering, national security and defense, with more potential applications that will be gradually exploited in the future [7,8].

In the past, the search for the auxetic effect has mainly focused on natural materials and specially designed structures in bulk form. In 1987, NPR behavior was discovered by Lakes in conventional low-density open-cell polymer foams. The key structural feature of these materials is that the ribs of cells permanently protruded inward [9]. Since then, NPR phenomena have been successfully found in many other bulk materials, including some cubic metals [10,11], α-cristobalite (SiO_2) [2], α-TeO_2 [12], the zeolite mineral natrolite [13], hard cyclic hexamers [14], metal-organic frameworks [15], and the folded Miura-ori structure [16,17]. Those auxetic behaviors in bulk materials are mostly attributed to peculiar reentrant or hinged geometric structures.

Due to their superior mechanical properties, two-dimensional (2D) auxetic materials offer opportunities to design nanoscale devices with specific functionalities and consequently have been subject to intensive research. Recently, the auxetic effect has been reported in several monolayer two-dimensional materials. Theoretical calculations and experiments confirmed that monolayer black phosphorene has an intrinsic auxetic effect [18,19], with a calculated Poisson's ratio of -0.027 in the out-of-plane direction [18]. Few-layer arsenic and borophane were predicted to have out-of-plane NPR as well [20,21]. Moreover, the in-plane NPR has been predicted in graphene [22], rippled graphene [23], two-dimensional silicon dioxide [24], pentagraphene [25,26], $h\alpha$-silica [27], Be_5C_2 [28], and some transition metal dichalcogenides [29]. The NPR effect of 2D materials usually originates from their unique puckered structures.

Most of the reported NPR 2D materials show a nearly invariable Poisson's ratio. Currently, the inability to tune the NPR values in these materials limits their usage in smart electromechanical devices, which have enormous potential for applications in various industrial fields and devices, including medicine, defense, and portable electronic devices. Such limitation could be attributed to the lack of knowledge about the relation between NPR and electronic structures of 2D materials. Indeed, previous studies mostly focused on how the puckered crystal structures affect the NPR [18,23]. Therefore, it is desirable to go one step further to obtain the essential understanding of the influence of electronic structures on NPR effects. That may provide effective ways to tune Poisson's

*junkai.deng@mail.xjtu.edu.cn
†zhe.liu@unimelb.edu.au

ratio via external stimuli, such as charging or electrical field. Such tunable NPR 2D materials would offer promising opportunities for smart device designs.

In this paper, using first-principles calculations, we find that negative Poisson's ratio generally exists in a set of group-IV monochalcogenide monolayers MX (M = Sn, Ge and X = S, Se). SnSe, GeS, and SnS have a negative out-of-plane Poisson's ratio in the armchair (x) tension. In contrast, GeSe has an NPR in the zigzag (y) tension. Our analysis shows that it is an intrinsic property for this type of material. The relationship between electronic structures and crystal structures is also established. We propose an effective electron doping method to fine tune the GeSe structure for a reversible and continuous change of ν_{zy} from -0.821 up to 0.895. In the end, we demonstrate the concept of strain engineering to tune the NPR of GeSe monolayer.

II. METHODS

Our first-principles calculations were carried out based on the density-functional theory (DFT), as implemented in the Vienna *Ab initio* Simulation Package (VASP) [30]. Electron exchange and correlation were described using the generalized-gradient approximation of the Perdew-Burke-Ernzerhof form [31], and projector-augmented wave potentials were used to treat core and valence electrons [32,33]. The monolayers were placed in the x-y plane. Periodic boundary condition was applied in all three directions. The cell has a length of 20 Å in the z direction to avoid the interactions between adjacent layers. To hold this interlayer space constant, the VASP source code was modified to allow the cells to relax within the x-y basal plane only. In all cases, the atoms were relaxed freely in all directions. An energy cutoff of 600 eV was chosen for the plane-wave basis set. All of the atoms in the unit cell were fully relaxed until the force on each atom was less than 0.001 eV/Å, ensuring the accuracy for the optimization of the structure. We have tested to ensure that the selected cutoff energy was sufficiently large for a well converged lattice constant value.

III. RESULTS AND DISCUSSION

The relaxed crystal structures of four group-IV monochalcogenide MX monolayers are shown in Fig. 1. All materials have puckered honeycomblike lattice similar to black phosphorene [34]. However, for SnS, SnSe, and GeS, the M atoms are located at the outmost layer of the puckered structure, while for GeSe, the outmost layer is occupied by the X atoms. We will show later that this subtle structural difference has a significant effect on Poisson's ratio of group-IV monochalcogenides. The armchair direction and zigzag direction of the lattice are defined as x and y coordinates, respectively. Unlike black phosphorene that only contains two atomic layers, each group-IV monochalcogenide monolayer MX contains four atomic layers stacked in the z direction, including two M atomic layers and two X atomic layers. Each M atom is covalently bonded to three neighboring X atoms and vice versa. The geometric anisotropy implies that these materials exhibit different mechanical response being subject to uniaxial loading in the x direction or the y direction. For a monolayer, the translational symmetry along the z direction is absent. We thus define the thickness of these materials as the vertical distance between the top and the bottom atomic layers.

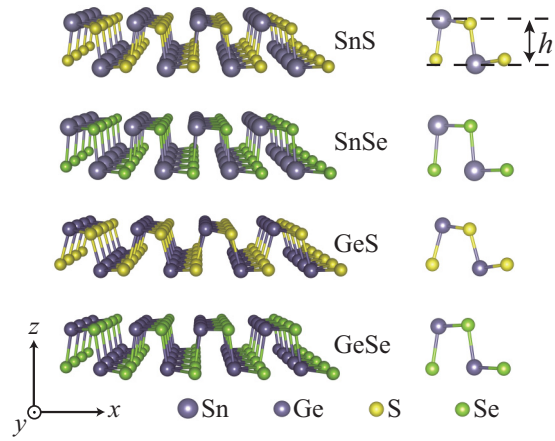

FIG. 1. Crystal structures of group-IV monochalcogenide (MX) monolayers. The atoms are distributed on four atomic layers. The thickness of these monolayers is defined as the vertical distance between the top and the bottom layers. From the side view, for SnS, SnSe, and GeS, group-IV atoms (M) are on the two outer layers, whereas for GeSe, chalcogen atoms (X) are on the two outer layers.

Next, we examine the structural response under uniaxial strain along the x or y direction and then calculate Poisson's ratios. Poisson's ratio is defined by $\nu_{ij} = -\partial\varepsilon_i/\partial\varepsilon_j$, where ε_j is the uniaxial strain applied in the j axis and ε_i is the resulting strain along the i axis. Figure 2 shows resulting strains in the two transverse directions under a uniaxial strain ε_x or ε_y in the range from -2% to 2%. Such a strain range is feasible in typical experimental measurements on 2D materials [35]. Good linear correlations are observed, and materials show NPR in the out-of-plane direction. In Fig. 2 , for SnS, SnSe, and GeS, under stretching in the x direction, their ε_z values remain positive and increase with increasing ε_x, indicating thickness enhancement. Thus, they have negative Poisson's ratios ν_{zx}. The similar relation is observed for GeSe but under uniaxial strain in the y direction. It has a negative ν_{zy} which is analogous to black phosphorene [18]. In addition, we find that in-plane Poisson's ratios ν_{xy} and ν_{yx} are all positive (Fig. 2).

Table I summarizes our results for calculated Poisson's ratios. Although the monochalcogenide monolayers possess similar structures to black phosphorene, the magnitudes of their NPR values are much higher than that of black phosphorene (-0.027) [18]. This reveals that they can have

TABLE I. Poisson's ratio results of group-IV monochalcogenide monolayers.

Materials	ν_{zx}	ν_{zy}	ν_{yx}	ν_{xy}
SnS	-0.004	0.404	0.422	0.961
SnSe	-0.210	0.352	0.423	0.851
GeS	-0.208	0.411	0.420	1.401
GeSe	0.583	-0.433	0.391	1.039

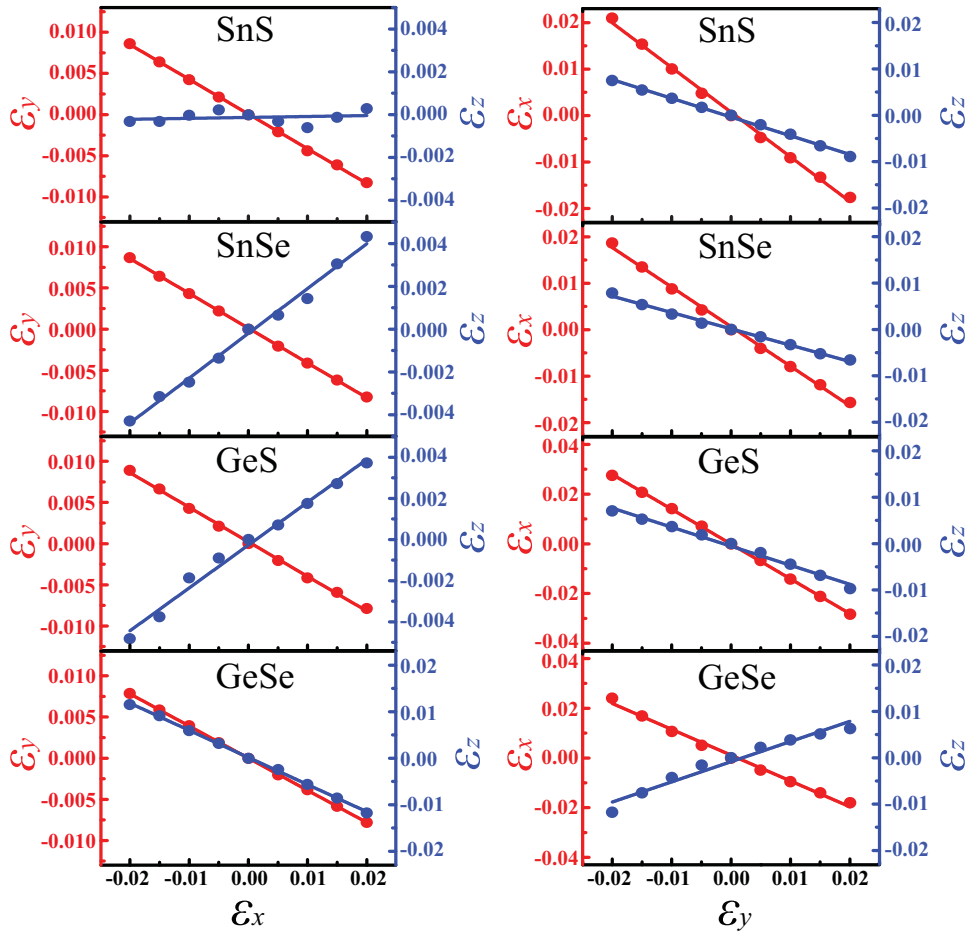

FIG. 2. The correlations between applied strain along the x (y) direction and two resultant transverse strains along the y (x) or z direction.

more sensitive thickness response under in-plane deformation. Particularly, GeSe monolayer has more significant out-of-plane NPR $\nu_{zy} \sim -0.433$. To our knowledge, it is the largest intrinsic NPR value among known pristine 2D materials [18,20–22,24,25,28,29,36–38]. Besides, in-plane positive Poisson's ratios ν_{xy} for these monochalcogenide monolayers are also larger than usual (0.5). That could be because they are very soft along the armchair direction due to the hingelike structure. Interestingly, GeSe and GeS have in-plane positive Poisson's ratios ν_{xy} even larger than 1. Gomes *et al.* reported a similar in-plane positive Poisson's ratio ν_{xy} for GeS [38]. It means that the transverse response strain ε_x has a larger magnitude than the applied longitudinal strain ε_y (Fig. 2). This property may have applications in strain amplifiers for functional nanodevices [39–43].

To understand the origins of the NPR of group-IV monochalcogenide monolayers, we examine the change of their crystal structures under uniaxial strain ε_x or ε_y. In Fig. 3(a), the black lines and red lines represent the variation of z coordinates of group-IV elements (M) and chalcogens (X) at the top two atomic layers respectively, under strain ranging from -0.02 to 0.02. The basis point ($z = 0$) is selected as the middle height of the monolayer. The black and red arrows in Fig. 3(b) depict the direction of motion for the X and M atoms under tensile strains of ε_x or ε_y. When the monolayers are stretched in the x direction, it is clear that the M atoms always move outward, while the X atoms move inward. The opposite directions of motion of the X and M atoms are characteristic of hingelike structures and can be explained as follows: it is well known that group-IV element materials are much stiffer than chalcogen materials [44]. Therefore, the change in the bond angle M-X-M is more significant under stretching along the x direction. As a result, the X atoms show an inward movement and the M atoms show an outward movement. When the monolayers are stretched in the y direction, it is equivalent to the lateral contraction in the x direction due to in-plane Poisson's effect as shown in Fig. 3(b). Consequently, the directions of motion of the M atoms and X atoms are reversed, i.e., the M atoms move inward and the X atoms move outward.

One can infer from Fig. 3(a) that for SnS, SnSe, and GeS monolayers, the M atoms are located at the two outmost atomic layers, since the z coordinates of the M atoms (black symbols) is larger than those of the X atoms (red symbols). The motion of the M atoms determines the change of thickness. As shown in Fig. 3(b), when stretched along the x direction, the M atoms move outward, leading to increasing ε_z and thus a negative Poisson's ratio ν_{zx}. When stretched along the y direction, the M atoms move inward, leading to decreasing ε_z and thus a positive Poisson's ratio ν_{zy}. However, GeSe monolayer shows a distinctive structural feature, i.e., the X (Se) atom located at the two outmost atomic layers.

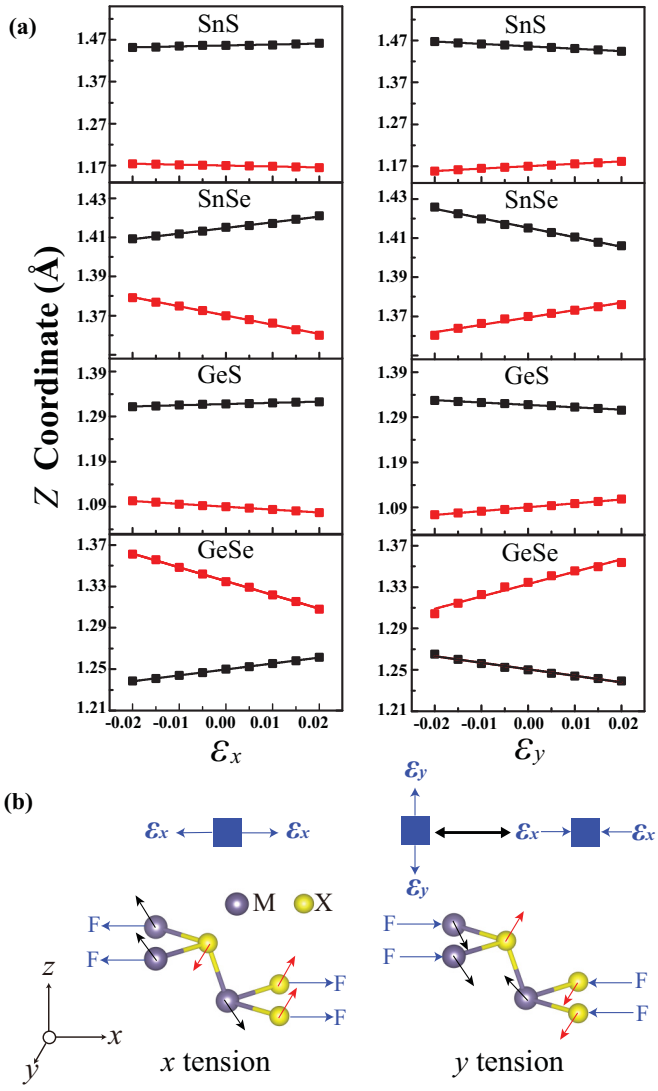

FIG. 3. (a) The motion of two atoms in the top two atomic layers under the strains in x or y direction. The black curves represent the z coordinates change of group-IV elements, and red curves represent the z coordinates change of chalcogens. The basis point (zero in z coordinates) is selected at the middle height of puckered crystal structures. (b) The black and red arrows depict the motion direction of the M and X atoms under tensile strains of ε_x or ε_y. The blue boxes show the strain conditions of these 2D materials. Note that stretching along the y direction is equivalent to contraction along the x direction because of Poisson's effect.

Therefore, GeSe shows the opposite sign of Poisson's ratio compared with the other three materials.

In order to explore the mechanism of the structural differences between GeSe and other MX monolayers, we analyze electronic structures of MX monolayers. As a prototypical example, Fig. 4(a) shows the projected electron density of states (PDOS) of GeS versus $E - E_f$, where E_f denotes Fermi level. Below -1.4 eV, DOS peaks for s orbitals and p orbitals show clear overlaps. Via inspection of the decomposed charge density, the overlaps stem from the covalent bonds connecting the M (Ge) and X (S) atoms. The electron-density distributions of GeS in the energy range from

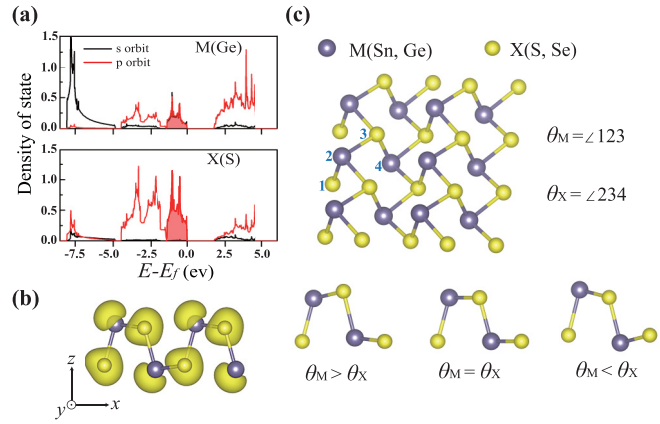

FIG. 4. (a) Projected electronic density of states (PDOS) for MX (GeS) from DFT calculation. The analysis in main text suggests that the M and X atoms undergo sp^3 hybridization. For each atom, three of the half-filled sp^3 orbitals form the covalent bonds connecting the M and X atoms. For both M and X, there is a lone-pair orbital (the shaded region). (b) Charge density of the lone-pair orbital on MX (GeS). The size of the lone-pair orbitals affects the tetrahedral bond angle θ_M and θ_X. (c) The relative magnitude of θ_M and θ_X leads to the three different puckered structures.

-1.4 to 0 eV are shown in Fig. 4(b). They appear like lone-pair orbitals. For the M (Ge) atom, it is s-p hybridization lone-pair orbital; for the X (S) atom, it is p-type lone-pair orbital. We can conclude that every M (Ge) and X (S) atom form three covalent bonds with its nearest-neighbor atoms and there is also a lone pair orbital for each atom. Figures 4(b) and 4(c) show that the three covalent bonds and lone pair orbital form a tetrahedral structure, suggesting a sp^3-like atomic orbital hybridization for Ge and S atoms.

As shown in Fig. 4(c), we have defined two bond angles θ_M and θ_X. These two bond angles should depend on the electronic structure, particularly the lone-pair electrons. For either group-IV or chalcogen atoms, moving down the periodic table, the lone-pair electron cloud will be more spread in space. It would force the three covalent bonds to bend downward, leading to smaller bond angles. This is consistent with our calculated angle values in MX crystals listed in Table II. Ge has a bond angle θ_{Ge} of 94–97°, whereas Sn has a bond angle θ_{Sn} within 89–92°. S has a bond angle θ_S of 101–105°, whereas Se has a smaller angle θ_{Se} about 94°. The difference between the bond angles of the M and X atoms is also noticeable. Generally, the X atoms have a larger bond angle than the M atoms ($\theta_X > \theta_M$). This could be attributed to its p-orbital-like lone pair. For example, compared with Ge

TABLE II. The tetrahedral angle θ_M and θ_X (Fig. 4) of the four MX crystals.

Materials	θ_X (degree)	θ_M (degree)
SnS	101.09	89.14
SnSe	94.22	92.44
GeS	105.18	94.74
GeSe	93.82	97.44

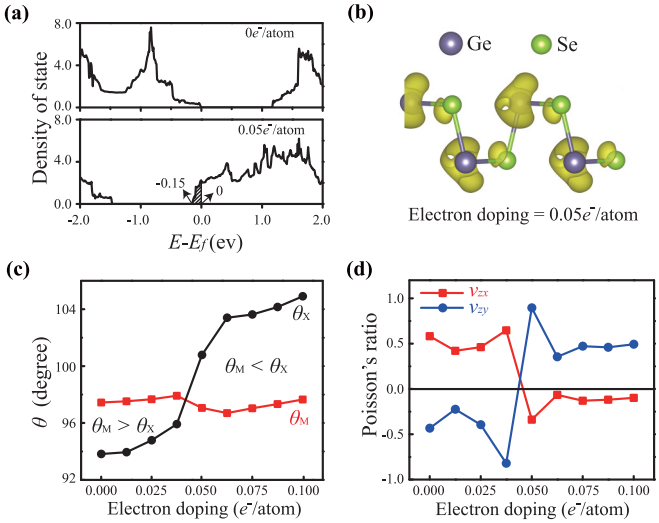

FIG. 5. Tunable Poisson's ratio of monolayer GeSe via electron doping engineering. (a) DOS (density of states) of GeSe with zero and $0.050e^-$/atom electron doping, respectively. The shaded region shows that the excess electrons located at the energy levels ranging from -0.15 to 0 eV (relative to Fermi level), which corresponds to the range from LUMO to LUMO + 0.15 eV in the zero electron doping case. (b) The distribution of doped excess electrons. (c) Electron doping leads to almost constant of θ_M and significant increase of θ_X. The crossover takes places at about $0.040e^-$/atom. (d) Poisson's ratio ν_{zx} (ν_{zy}) as a function of electron doping. They change sign from positive (negative) into negative (positive) arising from the crossover of the two angles in (c). See details in main text.

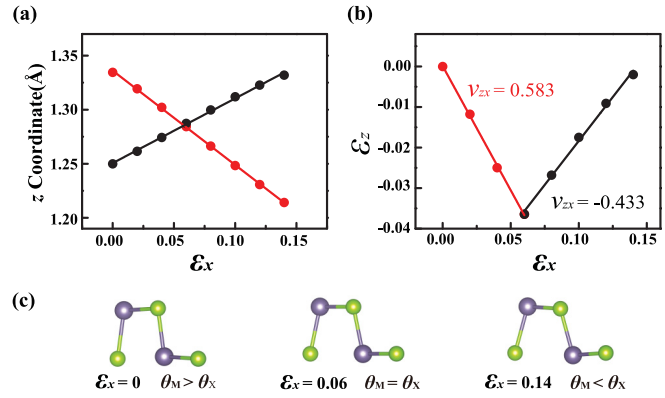

FIG. 6. Tunable Poisson's ratio ν_{zx} of monolayer GeSe via strain engineering in the x direction. (a) The z coordinates change of atom Ge (black line) and atom Se (red line), suggesting that the z coordinates of two atoms on the top two layers will be the same at $\varepsilon_x = 6\%$. (b) The transverse strain ε_z when GeSe is subjected to a strain ε_x in the range from 0 to 0.14. Poisson's ratio ν_{zx} changes from a positive value 0.583 to a negative value -0.433. (c) Cartoons to show the structural change of GeSe under different ε_x strains. There is a transition at $\varepsilon_x = 6\%$, corresponding to the intersection point of two lines in (a). The competition of bond angles θ_M and θ_X determines the sign of Poisson's ratio. See details in main text.

atoms, the lone-pair electrons are more uniformly distributed around S atoms [Fig. 4(b)]. There is less repulsion to push down the covalent bonds. But, if we choose an M atom in a top row and choose an X atom in a down row in the periodic table, the θ_X and θ_M could be comparable, e.g., GeSe, whose θ_X value can be smaller than θ_M.

Based on the comparison of θ_M and θ_X values, we have three different cases as illustrated in Fig. 4(c). Case I has $\theta_M > \theta_X$, where smaller θ_X causes the X atom located at the outmost atomic layers, e.g., GeSe. Case II ($\theta_M = \theta_X$) corresponds to a critical case where the X and M atoms are located on the same plane. The black phosphorene belongs to this case. Case III ($\theta_M < \theta_X$) corresponds to the other three materials, where smaller θ_M causes the M atoms to be located at the outmost atomic layers.

It should be noted that the physical origin of black phosphorene's NPR is different from the four materials in this paper. Its two bond angles remain equivalent even under strain conditions. That is because the two bond angles in phosphorene are constrained by chemical symmetry. Therefore, phosphorene can be regarded as a re-entrant structure involving two coupled orthogonal hinges [18]. This might be the reason for its relatively small NPR value (-0.027).

Our in-depth analysis of the electronic structure of MX shows that lone pair electrons play an essential role in the subtle difference between GeSe and other MX structures. For MX, both HOMO (highest occupied molecular orbital) and LUMO (lowest unoccupied molecular orbital) levels represent lone pair orbitals. It thus inspires us to propose electron doping as an effective way to tune the crystal structure and thus Poisson's ratio. Figure 5(a) shows the density of states (DOS) curves for GeSe monolayer with zero and $0.050e^-$/atom electrons doping, respectively. The excess doped electrons are occupied within the energy level ranging from -0.15 to 0 eV (Fermi level). This region corresponds to energy levels from LUMO to LUMO + 0.15 eV in the charge neutral case. The distribution of excess electrons is presented in Fig. 5(b), showing lone pair orbital features. Similar to Fig. 4, the doped electrons distribute around Ge atoms mostly in a region away from the three covalent bonds, whereas the distribution around the Se atom is more spherical with the highest density within the tetrahedron enclosed by the three covalent bonds. The different distributions around Ge and Se atoms (arising from their lone pair orbital differences in Fig. 4) should lead to different changes in the bond angles. As shown in Fig. 5(c), while the angle θ_M remains almost the same, the angle θ_X increases significantly upon electron doping. When the doped electron concentration exceeds 0.040 e^-/atom, θ_X becomes larger than θ_M. Consequently, as shown in Fig. 5(d), Poisson's ratio ν_{zx} (ν_{zy}) changes from a positive (negative) into a negative (positive) value. The tuning range of Poisson's ratio ν_{zy} is very large, from -0.821 to 0.895. Note that the maximum doping level of 0.100 e^-/atom corresponds to the area density of $2.35 \times 10^{14} e^-$ cm^{-2}, which is feasible in the experiments [45].

In addition to electron doping, we find strain engineering as another effective way to alter Poisson's ratio for GeSe monolayer. When stretching it along the x direction, the Se atoms move inward and Ge atoms move outward (Fig. 3). The thickness of GeSe reduces at small ε_x value thus showing a positive Poisson's ratio ν_{zx}. Further stretching along the x

direction to a critical point, the Se and Ge atoms would sit at the same atomic layer. Beyond this point, the Ge atoms are displaced to the outmost atomic layer. The outward motion of the Ge atoms then increases the thickness, leading to a negative Poisson's ratio ν_{zx}. Our DFT calculations verified our expectation. Figure 6(a) shows the change of z coordinates for the Ge atom and Se atom when GeSe is subject to uniaxial strain ε_x from 0 to 0.14. It is clear that the two lines meet at $\varepsilon_x = 0.06$. At this critical point, the Ge and Se atoms are on the same atomic plane. Poisson's ratio ν_{zx} exhibits a sudden change from 0.583 to −0.433 in Fig. 6(b). The structural distortion under ε_x is shown in Fig. 6(c). The competition between θ_M and θ_X determines the sign of Poisson ratio. We believe it is a general concept to tailor Poisson's ratio of these group-IV monochalcogenide monolayers through applying strain along a specific direction. Most interestingly, the group-IV monochalcogenides monolayers are known as piezoelectric 2D materials. Their giant in-plane piezoelectricity along the x direction suggests that the external electric fields can lead to tensile strains for group-IV monochalcogenides monolayers, thus changing Poisson's ratio [46].

IV. CONCLUSION

In summary, our DFT calculations demonstrate that group-IV monochalcogenide monolayers (SnS, SnSe, GeS, GeSe) generally have negative out-of-plane Poisson's ratio. The relative magnitudes of tetrahedra covalent bond angles θ_M and θ_X (for the M and X atoms respectively) determine either a M or X atom sitting at the outmost atomic layer. Then we can obtain either negative Poisson's ratio ν_{zx} or ν_{zy}, demonstrating the intrinsic auxetic property of group-IV monochalcogenide monolayers. Through the in-depth analysis of electronic structures, we further establish its relation to the crystal structure and demonstrate that doping electrons can effectively tune Poisson's ratio ν_{zy} of GeSe monolayer in a wide range from −0.821 to 0.895. We also propose to use strain engineering to tune Poisson's ratio of GeSe monolayer between two different values: 0.583 and −0.433. Such a tunable NPR 2D material would provide more design options and concepts in smart devices at small scale.

ACKNOWLEDGMENTS

The authors gratefully acknowledge the support of NSFC (Grants No. 51728203, No. 51471126, No. 51320105014, No. 51621063) and the support by 111 project 2.0 (Grant No. BP2018008). J.D. also thanks the support of the China Postdoctoral Science Foundation (Grant No. 2016T90911) and the Fundamental Research Funds for the Central Universities. J.Z.L. acknowledges the support from ARC discovery projects and HPC from National Computational Infrastructure from Australia. This work was also supported by State Key Laboratory for Mechanical Behavior of Materials and HPC platform of Xi'an Jiaotong University.

[1] M. D. Biegalski, K. Dörr, D. H. Kim, and H. M. Christen, Appl. Phys. Lett. **96**, 151905 (2010).
[2] A. Yeganeh-Haeri, D. J. Weidner, and J. B. Parise, Science **257**, 650 (1992).
[3] K. E. Evans, M. A. Nkansah, I. J. Hutchinson, and S. C. Rogers, Nature (London) **353**, 124 (1991).
[4] J. B. Choi and R. S. Lakes, J. Mater. Sci. **27**, 5375 (1992).
[5] R. S. Lakes and K. Elms, J. Compos. Mater. **27**, 1193 (1993).
[6] J. B. Choi and R. S. Lakes, Int. J. Fract. **80**, 73 (1996).
[7] F. Scarpa, IEEE Signal Process. Mag. **25**, 128 (2008).
[8] Y. J. Park and J. K. Kim, Adv. Mater. Sci. Eng. **2013**, 853289 (2013).
[9] R. Lakes, Science **235**, 1038 (1987).
[10] F. Milstein and K. Huang, Phys. Rev. B **19**, 2030 (1979).
[11] R. H. Baughman, J. M. Shacklette, A. A. Zakhidov, and S. Stafström, Nature (London) **392**, 362 (1998).
[12] H. Ogi, M. Fukunaga, M. Hirao, and H. Ledbetter, Phys. Rev. B **69**, 024104 (2004).
[13] J. J. Williams, C. W. Smith, K. E. Evans, Z. A. D. Lethbridge, and R. I. Walton, Chem. Mater. **19**, 2423 (2007).
[14] K. W. Wojciechowski, Mol. Phys. **61**, 1247 (1987).
[15] A. U. Ortiz, A. Boutin, A. H. Fuchs, and F. X. Coudert, Phys. Rev. Lett. **109**, 195502 (2012).
[16] Z. Y. Wei, Z. V. Guo, L. Dudte, H. Y. Liang, and L. Mahadevan, Phys. Rev. Lett. **110**, 215501 (2013).
[17] J. L. Silverberg, A. A. Evans, L. McLeod, R. C. Hayward, T. Hull, C. D. Santangelo, and I. Cohen, Science **345**, 647 (2014).
[18] J. W. Jiang and H. S. Park, Nat. Commun. **5**, 4727 (2014).
[19] Y. Du, J. Maassen, W. Wu, Z. Luo, X. Xu, and P. D. Ye, Nano Lett. **16**, 6701 (2016).
[20] H. Jianwei, X. Jiafeng, Z. Zhiya, Y. Dezheng, S. Mingsu, and X. Desheng, Appl. Phys. Express **8**, 041801 (2015).
[21] L. Kou, Y. Ma, C. Tang, Z. Sun, A. Du, and C. Chen, Nano Lett. **16**, 7910 (2016).
[22] J. W. Jiang, T. Chang, X. Guo, and H. S. Park, Nano Lett. **16**, 5286 (2016).
[23] H. Qin, Y. Sun, J. Z. Liu, M. Li, and Y. Liu, Nanoscale **9**, 4135 (2017).
[24] Z. Gao, X. Dong, N. Li, and J. Ren, Nano Lett. **17**, 772 (2017).
[25] H. Sun, S. Mukherjee, and C. V. Singh, Phys. Chem. Chem. Phys. **18**, 26736 (2016).
[26] S. Zhang, J. Zhou, Q. Wang, X. Chen, Y. Kawazoe, and P. Jena, Proc. Natl. Acad. Sci. U.S.A. **112**, 2372 (2015).
[27] V. O. Ozcelik, S. Cahangirov, and S. Ciraci, Phys. Rev. Lett. **112**, 246803 (2014).
[28] Y. Wang, F. Li, Y. Li, and Z. Chen, Nat. Commun. **7**, 11488 (2016).
[29] L. Yu, Q. Yan, and A. Ruzsinszky, Nat. Commun. **8**, 15224 (2017).
[30] G. Kresse and J. Furthmüller, Phys. Rev. B **54**, 11169 (1996).
[31] J. P. Perdew, K. Burke, and M. Ernzerhof, Phys. Rev. Lett. **77**, 3865 (1996).
[32] G. Kresse and D. Joubert, Phys. Rev. B **59**, 1758 (1999).
[33] P. E. Blöchl, Phys. Rev. B **50**, 17953 (1994).
[34] L. Kou, C. Chen, and S. C. Smith, J. Phys. Chem. Lett. **6**, 2794 (2015).

[35] P. Li, C. Jiang, S. Xu, Y. Zhuang, L. Gao, A. Hu, H. Wang, and Y. Lu, Nanoscale **9**, 9119 (2017).
[36] L. C. Zhang, G. Qin, W. Z. Fang, H. J. Cui, Q. R. Zheng, Q. B. Yan, and G. Su, Sci. Rep. **6**, 19830 (2016).
[37] S. Woo, H. C. Park, and Y.-W. Son, Phys. Rev. B **93**, 075420 (2016).
[38] L. C. Gomes, A. Carvalho, and A. H. Castro Neto, Phys. Rev. B **92**, 214103 (2015).
[39] Y. Huang, J. Liang, and Y. Chen, J. Mater. Chem. **22**, 3671 (2012).
[40] X. Yu, H. Cheng, M. Zhang, Y. Zhao, L. Qu, and G. Shi, Nat. Rev. Mater. **2**, 17046 (2017).
[41] H. Cheng, Y. Huang, G. Shi, L. Jiang, and L. Qu, Acc. Chem. Res. **50**, 1663 (2017).
[42] Z. Chang, J. Deng, G. G. Chandrakumara, W. Yan, and J. Z. Liu, Nat. Commun. **7**, 11972 (2016).
[43] J. Deng, Z. Chang, T. Zhao, X. Ding, J. Sun, and J. Z. Liu, J. Am. Chem. Soc. **138**, 4772 (2016).
[44] C. Kittel, *Introduction to Solid State Physics* (John Wiley and Sons, New York, 1986), p. 57, Table 3.
[45] D. K. Efetov and P. Kim, Phys. Rev. Lett. **105**, 256805 (2010).
[46] R. Fei, W. Li, J. Li, and L. Yang, Appl. Phys. Lett. **107**, 173104 (2015).